GEOPHYSICAL RESEARCH LETTERS, VOL. 36, L00B07, doi:10.1029/2008GL036689, 2009

Earthquake early warning system in southern Italy: Methodologies and performance evaluation

A. Zollo,[1] G. Iannaccone,[2] M. Lancieri,[2] L. Cantore,[1,3] V. Convertito,[2] A. Emolo,[1] G. Festa,[1] F. Gallovič,[1,4] M. Vassallo,[1,3] C. Martino,[1,3] C. Satriano,[1,3] and P. Gasparini[1,3]

Received 17 November 2008; revised 13 January 2009; accepted 15 January 2009; published 27 February 2009.

[1] We investigate the effect of extended faulting processes and heterogeneous wave propagation on the early warning system capability to predict the peak ground velocity (PGV) from moderate to large earthquakes occurring in the southern Apennines (Italy). Simulated time histories at the early warning network have been used to retrieve early estimates of source parameters and to predict the PGV, following an evolutionary, probabilistic approach. The system performance is measured through the Effective Lead-Time (ELT), i.e., the time interval between the arrival of the first S-wave and the time at which the probability to observe the true PGV value within one standard deviation becomes stationary, and the Probability of Prediction Error (PPE), which provides a measure of PGV prediction error. The regional maps of ELT and PPE show a significant variability around the fault up to large distances, thus indicating that the system's capability to accurately predict the observed peak ground motion strongly depends on distance and azimuth from the fault. **Citation:** Zollo, A., et al. (2009), Earthquake early warning system in southern Italy: Methodologies and performance evaluation, *Geophys. Res. Lett.*, *36*, L00B07, doi:10.1029/2008GL036689.

1. Introduction

[2] Earthquake Early Warning Systems (EEWS) are real-time information systems that are able to provide an alert on the potential damaging effects of an impending earthquake through the rapid telemetry and processing of data from dense instrument arrays deployed in the source region (regional systems) or in the site where the target to be protected is located (on-site systems) [*Kanamori*, 2005]. Following different technological and methodological approaches, prototypes or validated EEWS are currently operating in Japan, California (USA), Taiwan, Mexico, Turkey and Romania.

[3] In 2005, the development and implementation of a *regional* EEWS was started in southern Italy, based on a dense, wide dynamic seismic network deployed along the Apenninic belt region [*Weber et al.*, 2007], equipped with both acceleration and velocity sensors (see auxiliary material).[1] This is the region where large, destructive earthquakes in Italy have occurred during last centuries and there exist a significant probability for a $M > 5.5$ earthquake occurrence in the next decade [*Cinti et al.*, 2004].

[4] Methodologies for earthquake early warning assume a point-source model of the earthquake source and isotropic wave amplitude attenuation. These assumptions may be inadequate to describe the earthquake source and wave amplitude attenuation effects and they can introduce significant biases in the real-time estimation of earthquake location and magnitude. This issue is critically related to the EEWS performances in terms of expected lead-time (i.e., the time available for earthquake mitigation actions before the arrival of damaging waves) and of uncertainties in predicting the peak ground motion at the site of interest.

[5] The best practice would be to use the recordings of past strong earthquakes acquired at the network stations and, by means of an off-line analysis, to investigate the system capabilities to rapidly estimating the source parameters. This is not possible in the southern Apennines due to the relatively low seismicity rate in the magnitude range $M > 6$ and to the young age of the implemented EEWS. Therefore we adopted a different strategy, where the efficiency of early warning methodologies are investigated by the simulation of a large number of M6.9 and M6.0 earthquake scenarios, including the use of a standard 1-D Ground Motion Predictive Equation (GMPE) to predict the peak motion at distant sites.

2. Synthetic Waveforms and Earthquake Ground Motion Scenarios

[6] A massive synthetic waveform data-base has been produced for testing the performance of the southern Italy EEWS, using waveform play-back procedures which run off-line on simulated, synchronized earthquake records.

[7] The synthetic waveforms have been computed using the hybrid k-squared source model [*Gallovič and Brokesova*, 2007], which combines the integral approach based on the evaluation of the representation theorem for the low frequencies (<1 Hz) and the composite approach for the high frequencies (1–20 Hz). Both approaches are based on a common set of sub-sources providing "k-squared" slip distribution [*Herrero and Bernard*, 1994]. The source model is coupled with full-wavefield bedrock Green's functions for a 1D layered crustal model determined by the discrete wave-number method [*Bouchon*, 1981].

[1] Dipartimento di Scienze Fisiche, Università di Napoli "Federico II," Naples, Italy.
[2] Osservatorio Vesuviano, Istituto Nazionale di Geofisica e Vulcanologia, Naples, Italy.
[3] AMRA Scarl, Naples, Italy.
[4] Department of Geophysics, Charles University, Prague, Czech Republic.

0094-8276/09/2008GL036689$05.00

[1] Auxiliary materials are available in the HTML. doi:10.1029/2008GL036689.

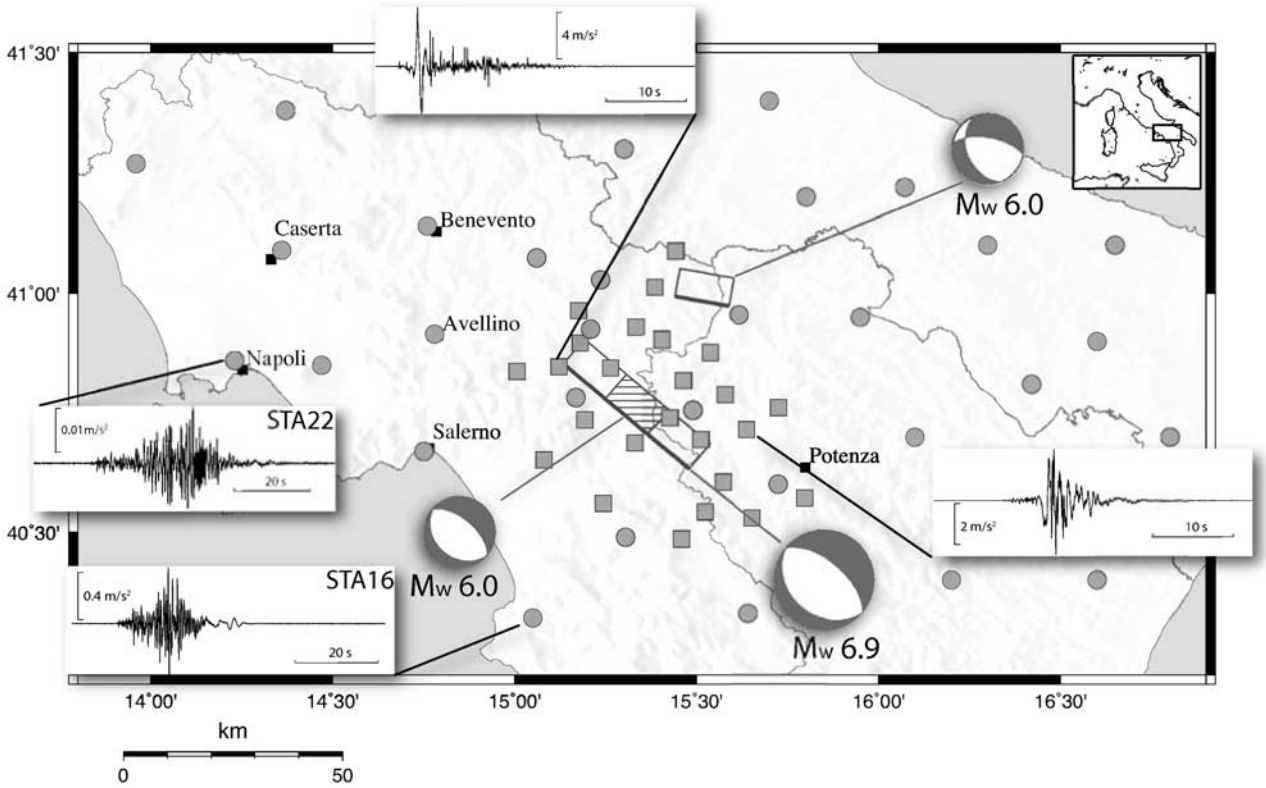

Figure 1. Acquisition layout of the numerical experiment for the evaluation of the EEW system performances and examples of synthetic accelerograms. Synthetic seismograms are computed at the early warning network (squares) and at a set of virtual stations (circles) in order to obtain a better coverage at regional scale. The locations of STA22 and STA16, whose PE plots are shown in Figure 2, are also indicated. The location, fault extent, focal mechanisms and moment magnitude of the simulated earthquakes are also shown.

[8] In this study we have simulated possible rupture scenarios for one M6.9 and two M6 earthquakes (Figure 1). The faults characteristics used for simulations are from the Italian active fault catalogue [*Basili et al.*, 2008]. The fault responsible for the main sub-event of the 1980 Irpinia earthquake is assumed as the source of the M6.9 earthquake. This fault is a NE dipping normal fault, striking along the Apennines direction (Figure 1). In the middle of the fault we assume a M6 event. The third M6 source is related to the causative fault of the 1930 earthquake that is a predominantly normal fault NE dipping located close to the north-eastern edge of the seismic network.

[9] The synthetic accelerograms corresponding to each earthquake scenario have been computed at the irregular grid of receivers shown in Figure 1. Only the ISNet stations are used for the real-time location and magnitude determination. For the Green's functions calculations, the 1D velocity model of *Improta et al.* [2003] is assumed.

[10] In total, 2 × 90 and 300 scenarios for the two M6 and the M6.9 earthquake, respectively, have been computed by considering variable nucleation points in the lower half of the fault, slip, and rupture velocity. The scenarios provide relatively large variability of the synthetics as illustrated in Figures 1 and 2. In order to make synthetic waveforms realistic in terms of ambient noise and site response, the records have been modified by adding synthetic noise as inferred from the observed power spectral density curves and by convolution with site transfer functions generated using the *Kennett*'s [1983] reflection matrix approach and P-, S-velocity and density profiles obtained from the Italian strong motion database (Working Group ITACA, 2008, http://itaca.mi.ingv.it).

3. Data Processing and Results

[11] We implemented a real-time, probabilistic evolutionary algorithm for early warning, whose main components are the automatic first-P picking, event location, magnitude estimation and prediction of ground motion intensity measure at a given target site.

[12] The automatic picks of P-arrival times on synthetic traces have been preliminarily carried out using a standard STA/LTA algorithm. The synthetic records have been filtered using a two poles, zero-phase shift Butterworth filter, in the frequency band 0.075–3 Hz following the processing scheme detailed by *Zollo et al.* [2006, 2007]. The three-component accelerograms have been double-integrated to obtain displacement and to evaluate the peak amplitude modulus in a time window Δt, as $PD = \max_{t \in Dt}\left(\sqrt{NS(t)^2+EW(t)^2+UD(t)^2}\right)$.

[13] At each second after the first automatically detected P-pick, the real-time location procedure proposed by *Satriano et al.* [2008] (RTLoc) is used to provide the hypocentral location, as soon as the first P–measurement is made available. Magnitudes are estimated from PD values in windows of 2 and 4 seconds for the P phase, and 2 seconds for the S phase following a Bayesian approach [*Lancieri*

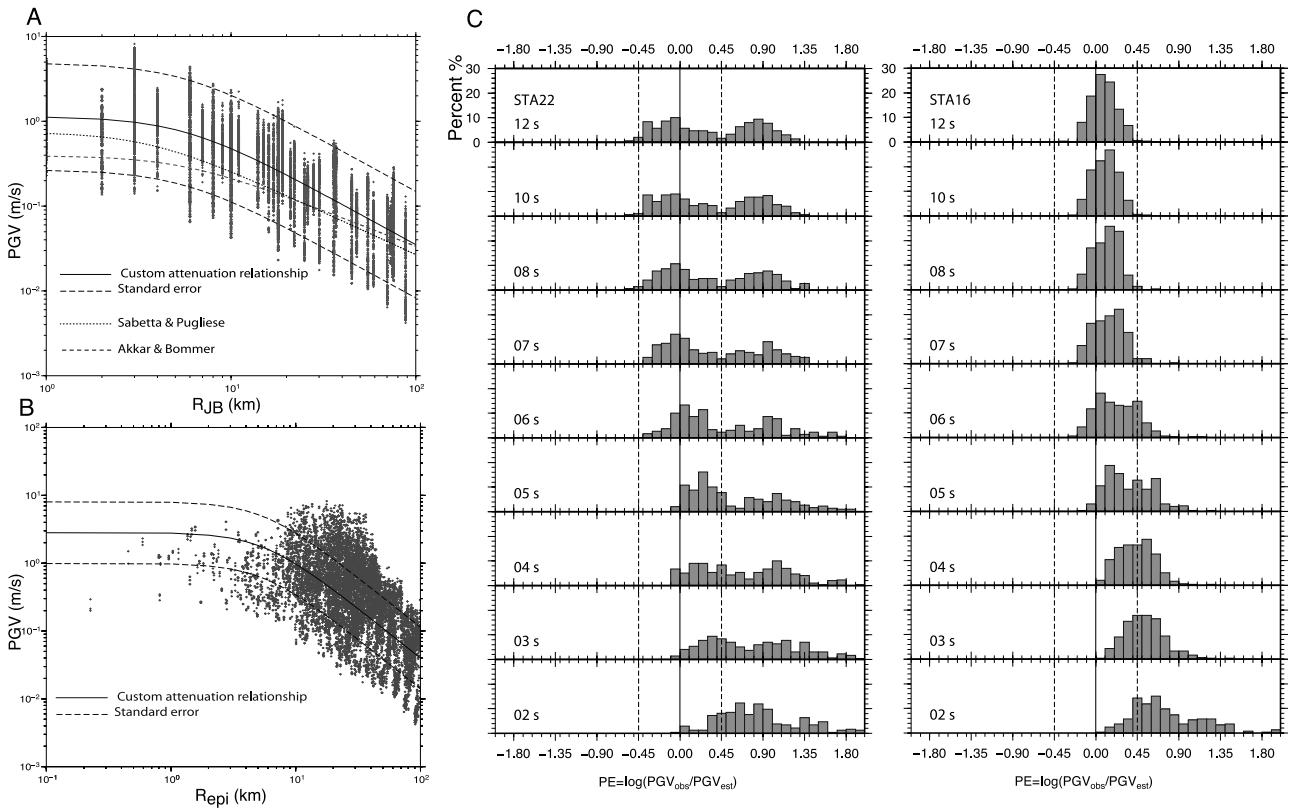

Figure 2. Comparison of synthetic PGV vs distance for various attenuation relationships assuming the M6.9 earthquake. (a) Synthetic database for PGV as function of the fault distance for the M 6.9 simulated earthquake. The GMPE for PGV (black line) has been obtained by measuring the peak (maximum between the two horizontal components) on synthetics and correlating to magnitude M and distance D, where D is defined as the minimum distance from the fault (Figure 2a) or the epicentral distance (Figure 2b). The dotted and dashed lines refer to the GMPEs proposed by *Sabetta and Pugliese* [1996] and *Akkar and Bommer* [2007], respectively. (b) Synthetic database for PGV as function of the epicentral distance for the M6.9 simulated earthquake. Black continuous line refers to the regression analysis performed in the present study, along with the estimated 1-sigma uncertainty bounds. The standard error value σ_E has been used in the definition of the Probability of Prediction Error (PPE) (see text). (c) Examples of PE distribution (see text for definition) vs time from the first P-arrival detected at the EW network at stations STA22 and STA16 (see Figure 1). The histograms are built based on synthetic accelerograms computed for 300 earthquake scenarios relative to an M 6.9 earthquake occurring inside the network. Ordinates are expressed in percent of the total number of scenarios. Dashed lines indicate the 1-sigma interval of the used GMPE.

and Zollo, 2008] (RTMag). PD values have been corrected for the distance attenuation and normalized at a reference distance of 10 km, based on a regression relationship between PD and magnitude and hypocentral distance obtained from synthetic waveforms.

[14] The earthquake location and magnitude parameters are used to predict the PGV at regional scale using the synthetic GMPE (Figure 2 and auxiliary material). Both representations in terms of the distance from the closest point of the fault and from the epicenter are shown in Figures 2a and 2b, the latter being used in the early warning methodology.

[15] At each second after the event origin and for each analyzed scenario, the earthquake location and magnitude predicted by the early warning procedures allows the estimation of i) the Maximum Lead-Time (MLT) (i.e., the delay of the S-phase arrival at the target with the time of first location and magnitude estimations), and ii) the Prediction Error on log(PGV), defined as PE = log (PGV^{obs}/PGV^{pred}), where PGV^{obs} is the PGV measured on the synthetic waveforms and PGV^{pred} is the value predicted by the EEWS using the synthetic GMPE model and the estimated earthquake location and magnitude.

[16] Furthermore, given the whole number of earthquake scenarios for a single earthquake, one can compute the distribution of parameter PE at each time step. Figure 2c displays examples of the evolutionary distribution of PE computed at two different sites for the M6.9 earthquake. The shape of the PE distribution depends on errors and failures on event identification and picking, on the complexity of the rupture process, on the number of stations used for early estimation of location and magnitude, and on the accuracy of the GMPE. The ideal distribution of the PE would be the one centered at 0 and having standard deviation smaller or comparable with that of the adopted GMPE model.

[17] Examples in Figure 2 indicate a time after the event origin, beyond which the distribution becomes stable, i.e., the addition of new observations does not change signifi-

cantly the distribution of PE, although its shape may differ from site to site.

[18] In general, the distributions in sites located along a direction orthogonal to the fault strike appear unimodal, while those for sites located along the strike direction are bimodal and show a larger dispersion. This can be attributed to persistent directivity effects contained in the simulated waveforms which, for some sites, cause data to be distributed symmetrically with respect to the GMPE that represents the median value.

[19] Following the example in Figure 2c, the Effective Lead-Time (ELT) at a given site can be defined as the time interval between the arrival of first S-wave and the time at which the distribution of parameter PE does not change with time. Denoting σ_E the standard deviation of the adopted GMPE model for PGV, we define the following stability criterion for PE distribution: given the range $[-\sigma_E; +\sigma_E]$ for the parameter PE, its distribution is stationary when the probability $P(PE \in [-\sigma_E; +\sigma_E])$ does not change significantly with time, i.e., less than 2%. We denote this probability as the Probability of Prediction Error (PPE), which is used, jointly with ELT, as an indicator of EEWS system performance, in terms of system capability to predict the strong motion parameter PGV, e.g., high values of PPE indicate acceptable system performances. Figure 3 shows the final results of EEWS performance analysis for a characteristic earthquake of M6.9 occurring inside the area covered by the seismic network. Results from simulations of M6 earthquakes occurring inside and at the border of the network are provided as auxiliary material. Concerning the event at the border of the network, we observe that the area with low values of PPE is larger while the ELT are generally smaller.

[20] The map of MLT and related variability are displayed in Figure 3a. A larger variability of parameter MLT is expected along the fault strike direction, because of the variability of rupture nucleation points along the fault. The MLT map should be directly compared with that of ELT (Figure 3b). The latter presents a shadow zone around the fault, having a radius of about 30 km, where we expect negative ELTs. It implies that for most scenarios the prediction of the PGV can be still improved as the magnitude value is updating: effectiveness of prediction inside the network may therefore depend on the specific source characteristics. As compared to the isotropic distribution of MLTs, the ELTs are on average 5s to 7s smaller, indicating that a value of magnitude for which the prediction becomes stable requires the P information from almost half of ISNet stations, with few of them already providing the 2s-S peak displacement. When comparing the ELT isolines to an isotropic distribution, we note a more pronounced elongation of ELT along the NW–SE, fault strike direction. Such a behavior can be related to the source radiation pattern and directivity, which are dominant along the fault strike direction with respect to other possible source complexities. Along the fault-strike direction the observed PGV is systematically higher than the predicted one and the probability to capture the true PGV (within one standard deviation) becomes quickly insensitive to improvements in the magnitude estimate.

[21] As concerns the distribution of parameter PPE (Figure 3c), smaller values are still concentrated in the fault strike direction and they can be ascribed to the dominant directivity effect as well as to wrong interpretation of the distance in the used attenuation law. The different station coverage, which are densely distributed in the Southern part of the fault, is the cause for higher values of PPE in the SE sector relative to NW. Finally PPE is high in the fault orthogonal direction, where large values indicate that the variability induced by finite fault effects is smoothed along this direction.

4. Discussion and Conclusions

[22] We have investigated the performance of the southern Italy EEWS in case of extended faulting processes occurring inside and at the border of the network. We have introduced the Effective Lead-Time, and the Probability of Prediction Error, the latter being an indicator of EEWS efficiency to predict the PGV. ELT shows a pronounced anisotropy along the fault-strike direction which is controlled by the focal mechanism and directivity. The map of PPE provides an image of the distribution of the prediction error related to different effects: network configuration, earthquake size and mechanism, attenuation relationship. In the analyzed case, it shows a larger variability around the fault, even at large distances, denoting the influence of rupture process complexity on EEWS capability to accurately predict the PGV at target sites.

[23] The map of PPE shows that systematic failures in PGV predictions may occur for sites located in or close to the fault strike direction, where observations are generally underestimated due to dominant directivity effects. As concerning the fault finiteness, the distance definition used for early warning needs to be revisited and the closest distance to the fault is likely to be the preferred distance in GMPE model. Improving the ground motion prediction of large earthquakes, at distances comparable with fault extension, requires the real time estimation of the fault geometry. The strike and slip can also be constrained 'a priori' by the tectonic context in which the earthquake occurs, while the fault extension can be related to the magnitude by empirical relationships [e.g., *Wells and Coppersmith*, 1994].

[24] The proposed methodology can be used to measure the performance of any operational EEWS, as well as a tool

Figure 3. Regional maps of Early Warning System performance indicators. The maps are computed for 300 earthquake scenarios for an M 6.9 occurring inside the network. See Figure 1 for earthquake location, fault extent and mechanism. (a) Distribution of average Maximum Lead-Time (MLT) in seconds (isolines) and the associated range of variation (grey shade). (b) Distribution of the Effective Lead-Time (ELT) in seconds. The shaded area inside the network indicates a zone with negative ELTs, where S-waves arrive before the distribution of PE becomes stable. (c) Distribution of PPE, the Probability of Prediction Error on parameter log (PGV) (see text for details). Shaded areas are obtained from a discrete representation of PPE, where lighter regions indicate a better efficiency of the EEWS to predict the PGV relative to darker regions.

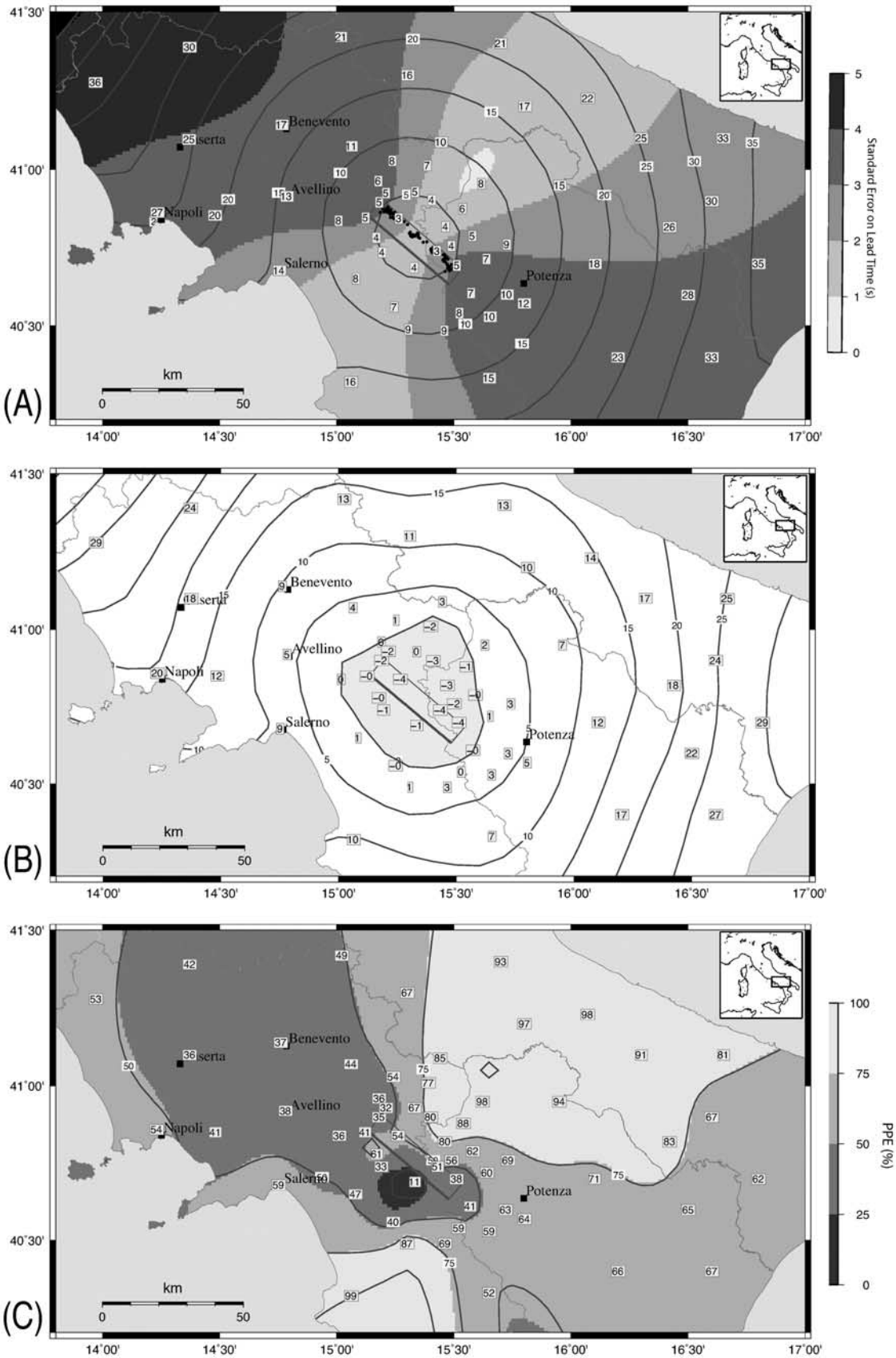
(A)
(B)
(C)
Benevento
Avellino
Salerno
Napoli
Potenza
serta
km
0
50
14°00'
14°30'
15°00'
15°30'
16°00'
16°30'
17°00'
41°30'
41°00'
40°30'
Standard Error on Lead Time (s)
PPE (%)

Figure 3

for designing the optimal station distribution, according to faults existing in a given area. The joint computation of ELT and PPE maps can be used to identify the potential applications of an EEWS as a function of distance from the earthquake causative fault. Based on the inventory of possible automated and individual actions to be performed in few tens of seconds preceding the arrival of strong shaking [e.g., *Goltz*, 2002], the ELT and PPE maps can serve to identify which targets can be protected (schools, hospitals, high speed trains, ...) and to design the adequate mitigation action, given the available time and probability of prediction error.

[25] Concerning the southern Italy EEWS the effectiveness of prediction depends on the specific scenario, whose real-time characterization becomes crucial for issuing an alert. As an example, for the densely populated Naples urban area, ELT can range between 8*s* and 16*s*, and PPE between 50% and 60%, indicating that several mitigation actions could be effective before S-waves shake the town.

[26] We finally remark that a fully functional seismic network has been assumed, although failures in the technological components (sensors, data-loggers and transmission system) may occur during a large earthquake. A complete analysis would therefore require an intersection of the prediction with the probability of missing data from few stations.

[27] **Acknowledgments.** We wish to thank the two anonymous reviewers for their useful comments and suggestions. This work was partially funded by AMRA scarl through the EU-SAFER project (contract 036935).

References

Akkar, S., and J. J. Bommer (2007), Empirical prediction equations for peak ground velocity derived from strong-motion records from Europe and the Middle East, *Bull. Seismol. Soc. Am.*, *97*, 511–530, doi:10.1785/0120060141.

Basili, R., G. Valensise, P. Vannoli, P. Burrato, U. Fracassi, S. Mariano, M. M. Tiberti, and E. Boschi (2008), The database of individual seismogenic sources (DISS), version 3: Summarizing 20 years of research on Italy's earthquake geology, *Tectonophysics*, *453*, 20–43, doi:10.1016/j.tecto.2007.04.014.

Bouchon, M. (1981), A simple method to calculate Green's functions for elastic layered media, *Bull. Seismol. Soc. Am.*, *71*, 959–971.

Cinti, F. R., L. Faenza, W. Marzocchi, and P. Montone (2004), Probability map of the next M $\geq$ 5.5 earthquakes in Italy, *Geochem. Geophys. Geosyst.*, *5*, Q11003, doi:10.1029/2004GC000724.

Gallovič, F., and J. Brokesova (2007), Hybrid k-squared source model for strong ground motion simulations: Introduction, *Phys. Earth Planet. Inter.*, *160*, 34–50.

Goltz, J. D. (2002), Introducing earthquake early warning in California: A summary of social science and public policy issues, technical report, Governor's Off. of Emergency Serv., Pasadena, Calif.

Herrero, A., and P. Bernard (1994), A kinematic self-similar rupture process for earthquakes, *Bull. Seismol. Soc. Am.*, *84*, 1216–1228.

Kanamori, H. (2005), Real-time seismology and earthquake damage mitigation, *Annu. Rev. Earth Planet. Sci.*, *33*, 195–214.

Kennett, B. L. N. (1983), *Seismic Wave Propagation in Stratified Media*, 342 pp., Cambridge Univ. Press, Cambridge, U. K.

Improta, L., M. T. Bonagura, P. Capuano, and G. Iannaccone (2003), An integrated geophysical investigation of the upper crust in the epicentral area of the 1980, M_s = 6.9, Irpinia earthquake (southern Italy), *Tectonophysics*, *361*, 139–169.

Lancieri, M., and A. Zollo (2008), A Bayesian approach to the real-time estimation of magnitude from the early *P* and *S* wave displacement peaks, *J. Geophys. Res.*, *113*, B12302, doi:10.1029/2007JB005386.

Sabetta, F., and A. Pugliese (1996), Estimation of response spectra and simulation of nonstationary earthquake ground motion, *Bull. Seismol. Soc. Am.*, *86*, 337–352.

Satriano, C., A. Lomax, and A. Zollo (2008), Real-time evolutionary earthquake location for seismic early warning, *Bull. Seismol. Soc. Am.*, *98*, 1482–1494, doi:10.1785/0120060159.

Weber, E., et al. (2007), An advanced seismic network in the southern Apennines (Italy) for seismicity investigations and experimentation with earthquake early warning, *Seismol. Res. Lett.*, *78*, 622–634.

Wells, D. L., and K. J. Coppersmith (1994), New empirical relationships among magnitude, rupture length, rupture width, rupture area, and surface displacement, *Bull. Seismol. Soc. Am.*, *84*, 974–1002.

Zollo, A., M. Lancieri, and S. Nielsen (2006), Earthquake magnitude estimation from peak amplitudes of very early seismic signals on strong motion records, *Geophys. Res. Lett.*, *33*, L23312, doi:10.1029/2006GL027795.

Zollo, A., M. Lancieri, and S. Nielsen (2007), Reply to comment by P. Rydelek et al. on "Earthquake magnitude estimation from peak amplitudes of very early seismic signals on strong motion records", *Geophys. Res. Lett.*, *34*, L20303, doi:10.1029/2007GL030560.

L. Cantore, A. Emolo, G. Festa, F. Gallovič, P. Gasparini, C. Martino, C. Satriano, M. Vassallo, and A. Zollo, Dipartimento di Scienze Fisiche, Università di Napoli "Federico II," via Cintia, I-80126 Naples, Italy. (aldo.zollo@unina.it)

V. Convertito, G. Iannaccone, and M. Lancieri, Osservatorio Vesuviano, Istituto Nazionale di Geofisica e Vulcanologia, via Diocleziano 328, I-80124 Naples, Italy.